Poly(ethylene glycol) functionalization of monolithic poly(divinyl benzene) for improved miniaturized solid phase extraction of protein-rich samples

Esme Candish, Aminreza Khodabandeh, Marianne Gaborieau, Thomas Rodemann, Robert A Shellie, Andrew A Gooley, Emily F Hilder

Poly(ethylene glycol) functionalization of monolithic poly(divinyl benzene) for improved miniaturized solid phase extraction of protein rich samples.

Esme Candish[1,2], Aminreza Khodabandeh[1], Marianne Gaborieau[3], Thomas Rodemann[4], Robert A Shellie[1], Andrew A Gooley[1,2], Emily F Hilder[1]*

[1]Australian Centre for Research on Separation Science, University of Tasmania, Private Bag 75, Hobart, Tasmania, Australia, 7001

[2]Trajan Scientific & Medical, 7 Argent Place, Ringwood, Victoria, Australia, 3134

[3] Western Sydney University, Molecular Medicine Research Group, Australian Centre for Research on Separation Science, School of Science and Health, Locked Bag 1797, Penrith, NSW, Australia, 2751

[4]Central Science Laboratory, University of Tasmania, Private Bag 74, Hobart, Tasmania, Australia, 7001

*Corresponding Author:

Tel: +61-8-8302 6292, Fax: +61-8-8302 0225

Email: emily.hilder@unisa.edu.au

Current address:

University of South Australia, Future Industries Institute, GPO Box 2471, Adelaide, SA, Australia, 5001

Abstract To improve the miniaturized solid phase extraction (SPE) of small molecules in protein rich samples biocompatible poly(divinyl benzene) (PDVB) monoliths were developed. Solid state ^{13}C NMR spectroscopy determined that the PDVB monolith possessed a significant fraction of residual vinyl groups (RVGs). The hydrophilic monomer poly(ethylene glycol methacrylate) (PEGMA) was grafted to the RVGs. Two PEGMA monomers, average M_n 360 and 950, were compared for graft solutions containing 5-20% monomer. Fluorescently labeled human serum albumin (HSA) was employed to probe non-specific protein binding. The intense fluorescent signal displayed by the PDVB was reduced for the optimized PDVB-*g*-$PEGMA_{360}$ (10%) and PDVB-*g*-$PEGMA_{950}$ (20%). The PEGMA content (w/w%) was quantified by solid state ^1H NMR to be 29.9 ± 1.6% for PDVB-*g*-$PEGMA_{360}$ and 7.7 ± 1.2% for PDVB-*g*-$PEGMA_{950}$. The anisole breakthrough curves of PDVB, PDVB-*g*-$PEGMA_{360}$ and PDVB-*g*-$PEGMA_{950}$ were compared. PDVB yielded a breakthrough volume (V_B) of 2.8 mL. Grafting the PDVB with $PEGMA_{360}$ led to a reduced V_B of only 0.5 mL and shallow breakthrough curve suggesting that PDVB-*g*-$PEGMA_{360}$ was not suitable for SPE. Conversely, for PDVB-*g*-$PEGMA_{950}$ the shape of the breakthrough curve and the V_B (2.3 mL) was maintained relative to PDVB. Both PDVB and PDVB-*g*-$PEGMA_{950}$ provided a high ibuprofen recovery of 92 ± 0.30% and 78 ± 0.93% respectively. The purification of ibuprofen from human plasma was compared for PDVB and PDVB-*g*-$PEGMA_{950}$. Extracts were analyzed by at-line electrospray ionization mass spectrometry (ESI-MS). The ESI-MS assay for PDVB-*g*-$PEGMA_{950}$ demonstrated a greater sensitivity than PDVB indicating that PDVB-*g*-$PEGMA_{950}$ provided a superior analyte purification.

Keywords sample preparation; porous polymer monolith; solid phase extraction; grafting; biocompatible; mass spectrometry

Introduction

The highly selective and sensitive analysis of drugs and metabolites by mass spectrometry (MS) has emerged as an essential tool in many fields including clinical chemistry, forensic toxicology and pharmaceutical research. Blood, plasma and serum are among the most difficult samples to analyze as they are poorly compatible with MS [1]. Matrix components, including cellular material, proteins and non-volatile lower molecular weight solutes can severely reduce assay sensitivity by suppressing the electrospray ionization (ESI) of the analyte [2]. Furthermore, matrix components will complicate data and foul the instrumentation. The key to achieving a highly sensitive and accurate analysis is to present a purified sample to the MS.

Preparing a sample for analysis is labor intensive and time consuming, often taking over 80% of the total analysis time [3]. Fortunately, rapid workflows can be achieved using miniaturized solid phase extraction (SPE). Hydrophobic and ion-exchange adsorbents are extremely efficient for removal of salts and non-adsorbed matrix compounds but protein rich matrices remain problematic. Proteins exhibit both hydrophobic and ionic interactions resulting in their non-specific adsorption and precipitation on solid surfaces [4]. Non-specific protein adsorption will foul the adsorbent bed, leading to a diminished extraction performance and a reduced assay sensitivity [4, 5]. In addition, protein fouling often leads to the blockage of the SPE cartridge, which can result in sample wastage. Therefore, additional labor intensive and time consuming sample pretreatment procedures including centrifugation, protein precipitation and filtration are routinely introduced into the workflow prior to SPE. Alternatively, the morphology and chemistry of the SPE adsorbent can be engineered to improve biocompatibility by reducing the non-specific adsorption of proteins.

Restricted access materials (RAM) can facilitate the rapid and efficient purification of biological samples; both non-adsorbed low molecular weight compounds and the protein rich matrix can be eliminated using a single adsorbent [6-10]. A diffusion barrier (physical or chemical) limits the accessibility of proteins to the adsorbent's surface. We have recently demonstrated that large surface area polymer monoliths adsorbents based on poly(divinyl benzene) (PDVB) are highly promising for the size selective sample clean-up of small molecules [11]. Inherent micro- (0.2-2 nm) and mesopores (2-50 nm) present a physical barrier, which dictates that larger matrix components pass through the adsorbent bed unretained, thus producing more purified extracts. Unfortunately, the hydrophobic nature of the PDVB remains problematic for protein-rich samples. Scope exists to reduce the non-specific surface adhesion of proteins by introducing surface functionality that act as a chemical barrier [12-14].

To achieve the unique pore structure of the PDVB adsorbent it is necessary to fabricate from a high concentration of crosslinking monomer. Therefore, approaches to introduce a chemical barrier are limited to a post-polymerization reaction whereby a layer is grafted to the adsorbent surface [15, 16]. It is well established that grafting the monomer poly(ethylene glycol) methacrylate (PEGMA) onto a hydrophobic surface results in a reduction of non-specific proteins binding through a combination of the hydrophilicity and the steric hindrance imparted by the long PEG chains [17, 18]. Grafting reactions undertaken thermally often exploit the residual reactive initiators, employed for living/controlled polymerizations, as attachment points for further functionalization [10, 19, 20]. Unfortunately, this approach often necessitates specialized initiators and the conditions of polymerization can be limited. A simpler protocol involves utilizing the residual vinyl groups (RVGs) of the PDVB that remain

unreacted for further functionalization [21-23]. Gaborieau *et al.* determined that PDVB particulate can possess 39-43% accessible RVGs that are available for further functionalization [23]. The purpose of the current study was to develop an approach for the PEGMA grafting of PDVB adsorbents using the RVGs. Grafted adsorbents were optimized to reduce non-specific protein interactions while preserving hydrophobic capacity and analyte interactions. Grafting was characterized using scanning electron microscopy (SEM), non-specific protein binding, solid-state nuclear magnetic resonance (NMR) spectroscopy and frontal analysis. The suitability of the resulting adsorbent was demonstrated for the improved miniaturized SPE purification of highly complex, protein rich, biological samples prior to MS.

Experimental section

Chemicals and materials

DVB (containing 80% 1,3-DVB + 1,4-DVB and 20% 1-ethyl-3-vinylbenzene + 1-ethyl-4-vinylbenzene), poly(ethylene glycol) methyl ether methacrylate average M_n 950 ($PEGMA_{950}$), poly(ethylene glycol) methacrylate average M_n 360 ($PEGMA_{360}$), poly(ethylene glycol) diacrylate average M_n 258 ($PEGDA_{258}$), anisole, 1-dodecanol, benzophenone (99%), ibuprofen, human serum albumin (HSA) lyophilized powder ≥97%, fluorescamine, ammonium hydroxide and sodium tetraborate were all purchased from Sigma Aldrich (Castle Hill, Australia). The monomer inhibitors were removed using a packed bed of basic alumina. The initiator, 2,2'-azo-bis-isobutyronitrile (AIBN), was obtained from MP Biomedicals (Santa Ana, CA, USA) and purified by recrystallization with methanol. The high performance liquid chromatography (HPLC) grade solvents; acetone, acetonitrile, methanol and toluene were all purchased from Sigma Aldrich. The water was purified with a Milli-Q

system (Millipore, Bedford, MA, USA). Polyethylene (PE) tubing (1.57 mm i.d.) was obtained from SDR Scientific (Chatswood, Australia). The MEPS cartridge assembly included frits, shank and needle hub components (SGE Analytical Science, Ringwood, Australia).

Sample collection

Blood samples were obtained by finger lancet (Acc-Chek Softclix, Roche Diagostics, Castle Hill, Australia) from a healthy female volunteer and stored in EDTA miniCollect tubes (ThermoScientific, Scoresby, Australia). All blood samples were centrifuged to obtain the plasma fraction. The plasma was diluted with water (20% v/v) and spiked with 50 ng mL^{-1} ibuprofen.

Instrumentation

An inverted fluorescence microscope (Nikon, Eclipse Ti-U, Japan) was employed to determine protein adsorption with the violet pass excitation (lex at 380-420 nm) and emission (lem at 450 nm) filters (Semrock, Rochester, NY, USA). The microscope was operated with NIS-Elements BR 3.10 software (Melville, NY, USA).The Brunauer–Emmett–Teller (BET) surface area and microporosity were assessed by argon adsorption/desorption at 77 K using a Tristar II analyzer (Particle and Surface Science, Gosford, Australia). Microporous surface area was determined using t-plots and the pore size was assessed using the non-localized density functional theory (NLDFT). The macroporous properties of the adsorbent materials were measured using an Autopore IV mercury intrusion porosimeter. The surface morphologies of the adsorbents were analyzed using a Hitachi SU-70 field emission SEM, the polymer monoliths were sputter-coated with platinum.

The chemical functionality of the adsorbents was determined using solid-state ^{13}C cross-polarization magic angle spinning (CP-MAS) NMR spectroscopy, ^{1}H MAS NMR spectroscopy and attenuated total reflectance fourier transform infrared (ATR-FTIR) spectroscopy. ^{13}C CP-MAS NMR was carried out to determine the presence of vinyl groups on the PDVB using a Bruker DPX 200 spectrometer (Bruker, Alexandria, Australia) operating at 50 MHz Larmor frequency for ^{13}C, using a 4 μs 90° pulse, a 4 ms contact time, a 3 s repetition delay, and 15 360 transients. ^{13}C CP-MAS NMR carried out to determine the presence of PEGMA in the PDVB utilized a Bruker DRX 300 spectrometer operating at 75 MHz Larmor frequency for ^{13}C, using a 5 μs 90° pulse, a 4 ms contact time, a 3 s repetition delay, and 13 112 to 16 472 transients. Quantitative ^{1}H MAS NMR spectra of the grafted samples were recorded on a Bruker DRX 300 spectrometer at 300 MHz Larmor frequency for ^{1}H, using a 10 μs 90° pulse, a 10 s repetition delay, and 64 transients. In order to determine true relative signal integrals it was checked that the magnetization was fully recovered between pulses for ^{1}H NMR signals of both PDVB and PEGMA (**Section S5**) [24]. All experiments were carried out with 4 mm solid-state MAS NMR probeheads at a MAS rotational frequency of 10 kHz. ^{1}H and ^{13}C pulses were calibrated with adamantane and a mixture of 3 singly ^{13}C labeled alanines. The ^{13}C chemical shift scale was externally referenced to tetramethylsilane at 0.0 ppm using adamantane by setting the CH resonance to 38.5 ppm [25]. All data was collected using Topspin software (Bruker, Alexandria, Australia). ATR-FTIR spectroscopy was used to determine the functional groups of the adsorbents. The spectra were recorded on a Vertex 70 spectrometer (Bruker Optic, Ettlingen, Germany) in the 500–4000 cm^{-1} region, 32 scans were signal-averaged with a spectral resolution of 4 cm^{-1} using a

single reflection diamond ATR attachment, Platinum ATR (Bruker Ettlingen, Germany).

Miniaturized SPE adsorbent performance was assessed using an ICS3000 system (ThermoScientific, Scoresby, Australia) consisting of two quaternary solvent pumps, an autosampler and an ultraviolet (UV) detector. Analyte recovery and protein adsorption from the offline SPE extraction was analyzed using a ProteCol C8 (3 µm particles and 1000 Å pores, 4.6 mm i.d. × 250 mm) HPLC column (SGE Analytical Science, Ringwood, Australia). A gradient elution was used with mobile phase A (95:5 0.1% trifluoroacetic acid:methanol) (v/v) and mobile phase B (95:5 methanol: 0.1% trifluoroacetic acid) (v/v). The elution involved ramping from 60% mobile phase A to 100% mobile phase B in 10 min at a flow rate of 600 µL min^{-1}. For miniaturized SPE, all MEPS assemblies comprised a cartridge coupled to 100 µL or 50 µL controlled directional flow (CDF)-MEPS syringe driven by a hand held semi automated analytical syringe driver (eVol, SGE Analytical Science, Ringwood, Australia).

MS experiments were performed using a micrOTOF-Q MS (Bruker, Preston, Australia) equipped with an ESI source. The instrument was operated as follows: +3.5 kV capillary potential (negative ion mode), nitrogen nebulizer gas at 1.7 bar, nitrogen dry gas at 220°C and a flow rate of 4 L min^{-1}. Calibration of the TOF-MS was carried out prior to each analysis by direct infusion of the low concentration multimode tune mix (Agilent Technologies, Mulgrave, Australia) at 5 µL min^{-1}. Data was collected using micrOTOF control 2.2 with a mass range of 100 - 600 m/z at an acquisition rate of 0.5 Hz. Ibuprofen was monitored using the extracted ion 205.12 ±0.01 m/z. The

analyte identity was confirmed using standard addition. All ion traces were processed using Compass Data Analysis 4.0 (Bruker, Preston, Australia) and smoothed using the Gauss smoothing algorithm at 2.003 s.

Preparation of the monolithic SPE adsorbents

The fabrication of PDVB adsorbents was based on an approach described by Sýkora *et al*. [26]. Briefly, the composition included 40% w/w DVB, 8% w/w toluene, 52% w/w 1-dodecanol and 1% w/w (with respect to the monomer) AIBN. All polymerization mixtures were prepared in glass vials, sonicated for 2 min then purged with nitrogen for 10 min. Polymerization reactions were carried out at 70 °C for 180 min. Monolithic adsorbents were prepared in bulk and is PE tubing. Any residual polymerization mixture was removed by Soxhlet extraction with methanol for 24 h. The adsorbents were then dried overnight under vacuum at 25 °C.

The post-polymerization thermal grafting reaction was developed from an approach described by Tripp *et al.* [22]. The grafting mixture was prepared in toluene containing 5-20% w/w functional monomer ($PEGMA_{360}$ or $PEGMA_{950}$), 1% w/w of the crosslinking monomer, $PEGDA_{258}$, and 1% w/w AIBN. The bulk monolith was submerged in the grafting mixture, while the PE tubes containing monolith were manually flushed with grafting mixture then submerged in the grafting solution. The mixture was polymerized at 65°C for 20 h. The products were Soxhlet extracted with methanol for 24 h and dried under vacuum overnight.

For testing the MEPS format was explored, MEPS cartridges were filled with monolith weighing 2 ± 0.2 mg. Once assembled the cartridges were flushed with 20 mL of 95:5 methanol:water (v/v).

Fluorescence assay of protein adsorption

To determine HSA adsorption, a stock solution of the protein was prepared at 1 mg mL^{-1} in 10 mM sodium tetraborate buffer. A 3 mg mL^{-1} solution of fluorescamine in acetone was prepared. A final protein concentration of 50 μg mL^{-1} was achieved by combining 5% HSA solution and 15% fluorescamine solution in a 10 mM sodium tetraborate buffer. Adsorbents were first conditioned with 250 μL of methanol and equilibrated with 250 μL of water at 50 μL min^{-1}. A 400 μL aliquot of the protein solution (50 mg L^{-1} HSA) was passed through the adsorbent and any unretained protein was flushed out with 250 μL of water, a flow rate of 50 μL min^{-1} was used. The fluorescence intensity of the cross-section of the adsorbent was analyzed. The signal of each adsorbent was compared with the corresponding blank (adsorbents imaged prior to the protein-binding assay **Section S4**).

Adsorbent performance for SPE

Breakthrough times and adsorption behavior for the SPE adsorbents were determined using frontal analysis. The MEPS cartridge was inserted between the dual quaternary pump and the UV detector. Pump 1 delivered the solvent solutions while Pump 2 delivered the aqueous analyte solution. The adsorbent was first conditioned with 2.5 mL of methanol:water (95:5 %v/v) using a continuous flow of 1 mL min^{-1} then equilibrated with 2.5 mL water:methanol (95:5 %v/v) at the same flow rate. The probe analytes, anisole (100 mg L^{-1}) and ibuprofen (10 mg L^{-1}), were employed. A

lower concentration of ibuprofen was employed due the lower aqueous solubility. The analyte in aqueous solution was continuously pumped over the adsorbent bed and the cartridge effluent was monitored at 254 nm. Uracil was employed to determine the void volume of the system (including cartridge). Each analysis was undertaken in duplicate. Backpressure of SPE cartridges was monitored to determined permeability.

Analyte recovery and protein adsorption for the SPE adsorbents was determined by offline SPE. The processed extracts were analyzed by HPLC-UV to determine peak area. The SPE cartridge was attached to a 100 µL CDF-MEPS syringe (a modified MEPS needle [27]), sample and solvent were aspirated into the syringe barrel with the valve in Position 2 and dispensed with the valve in Position 1. In all cases the flow rate to aspirate was 3.5 mL min^{-1} while dispensing was achieved at 1.0 mL min^{-1}. To determine the protein adsorption of the SPE adsorbents the extraction workflow involved preconditioning the adsorbent with 100 µL of methanol and then 100 µL of water. Next, a 100 µL aliquot of HSA (1000 mg L^{-1} aqueous solution) was passed through the adsorbent bed. To assess the depletion of the HSA the effluent was collected and compared with a non-extracted HSA solution (n=3). To determine analyte recovery the adsorbent was conditioned and equilibrated as above with methanol and water respectively. Next, a 100 µL aliquot of the 10 mg L^{-1} ibuprofen in aqueous solution was applied to the adsorbent, then any unretained compounds were removed with 100 µL of water. The analyte was eluted with 100 µL of methanol and extracts were analysed by HPLC-UV (n=3). The recovery was determined by comparing the peak area for an extracted ibuprofen solution with a non-extracted ibuprofen sample. For the MS analysis the 50 µL CDF syringe was employed. The sample was processed as above. The elution solvent employed was acetonitrile with 0.3% v/v ammonium hydroxide. The processed sample was delivered directly to the

ESI source at a flow rate of 20 μL min^{-1} (n=3). Following the first elution a second 50 μL elution was performed using 1% formic acid:isopropanol (60:40 %v/v) to clean the bed.

Results and discussion

Characterization of the PDVB adsorbent

The desirable attributes of an adsorbent for the rapid and efficient miniaturized SPE of protein rich biological samples are: high permeability, large surface area and biocompatibility. For fast SPE workflows, large macropores are favorable to ensure maximum flow rates can be employed. The macroporous properties of the PDVB were investigated using mercury intrusion porosimetry. The PDVB adsorbent presents a large macropore size of 6.7 μm, this infers a highly permeable morphology. The permeability was measured using an HPLC pump and the pressure-drop across the device was determined. The permeability of the PDVB adsorbent was estimated to be 6.7×10^{-15} m^2 (23% propagated error).

For a sensitive assay a large surface area is desirable, as extraction capacity is strongly related to the interactable surface. SEM provides a visual assessment of the clustered interconnected globules of the PDVB adsorbent (**Figure 1A**). Agglomerates of 5–10 nm microspheres roughened the surface of the interconnected globules. The specific surface area of PDVB was determined to be 497 mg g^{-1} by argon adsorption/desorption. The PDVB isotherm presents a combination of a *Type I* isotherm and a *Type IV* isotherm, indicative of micro- and mesopores respectively (**Figure 1B**). The *Type H2* hysteresis loop suggests the mesopores are small and exist over a broad distribution in sizes and shape. NLDFT confirms these pores range from 1 to 6 nm, but the vast majority are micropores of less than 2 nm (**Figure 1C**). The slope of the t-plot suggests that 93% of the total pore volume (0.30 cm^3 g^{-1}) is attributed to the micropores (0.28 cm^3 g^{-1}). Only a small percentage of the surface area (16 mg g^{-1}) can be attributed to the external surface. The innate process of

303 fabricating PDVB monoliths creates a physical size exclusion barrier that inhibits
304 proteins from gaining access to the large internal surface. However the external
305 hydrophobic surface remains problematic for protein fouling of the PDVB.
306
307 **Figure 2** shows the solid-state ^{13}C CP-MAS NMR spectra of the PDVB, the chemical
308 shift assignment is depicted in **Scheme 1.** Greater detail of the complete chemical
309 shift assignments can be found in **Table S1**. The strong signals at 138 and 113 ppm
310 (signals B and D) correspond to vinyl carbons adjacent and non-adjacent to the
311 aromatic ring. Even though this NMR measurement is not quantitative, the strong B
312 and D signals indicate the presence of unreacted vinyl groups on a significant fraction
313 of the monomer units [23]. Some of these RVGs will be present in the internalized
314 structure and unavailable for modification; the others are available for the grafting of
315 a chemical barrier to restrict non-specific protein interactions.
316
317 *PEG functionalization of PDVB adsorbents*
318 The hydrophilic monomer, PEGMA, was selected for grafting as it can be covalently
319 attached to the adsorbent's surface *via* a free radical polymerization [4, 17]. The
320 mechanism of protein resistance is believed to be a combination of the hydrophilic
321 glycol groups and the steric hindrance imparted by the long PEG chains. We chose to
322 explore two different PEGMA monomers with average molecular weights of M_n 360
323 and 950 g mol^{-1}. To achieve grafting, the preformed PDVB was submerged in a
324 solution containing 5-20% of the PEGMA monomer and 1% of the crosslinking
325 monomer, $PEGDA_{258}$, in toluene. Polymerizations containing 10 and 20% $PEGMA_{360}$
326 in the graft solution yielded a sticky transparent gel. For this reason higher

concentrations of PEGMA were not explored for either of the monomers. Following polymerization, the graft solution of $PEGMA_{950}$ (all concentrations) remained liquid.

Characterization of the PEGMA grafted PDVB adsorbents

To achieve successful miniaturized SPE it is critical that the analyte is able to quickly and efficiently interact with the adsorbent. Therefore, the hydrophilic layer must be carefully optimized, as it should be appropriately dense to prevent proteins from accessing the hydrophobic surface but it also must remain sufficiently thin and permeable to ensure that the analyte can efficiently interact with the hydrophobic inner surface [28-30]. The adsorbents were visually inspected using SEM to determine the presence of the grafted PEGMA (**Figure 3**). The grafted layer was clearly evident for adsorbent prepared using 20% and 10% $PEGMA_{360}$ in the graft solution. The PDVB-*g*-$PEGMA_{360}$ prepared with 20% $PEGMA_{360}$ displayed a thick coating of the grafted layer which masked the globular features that are characteristic of the PDVB scaffold (**Figure 1A**). The thickness of the $PEGMA_{360}$ layer raised concern over the suitability of this adsorbent for miniaturized SPE, thus PDVB-*g*-$PEGMA_{360}$ (20%) was not assessed further. The lower concentration of 10% $PEGMA_{360}$ in the graft solution yielded a thinner sheet like layer which draped the polymer globules of the PDVB. On the other hand, the adsorbent prepared from 5% $PEGMA_{360}$ in the graft solution showed no evidence of a PEGMA graft layer, appearing identical to the PDVB scaffold (**Figure 1A**). Additional SEM images over wider range of magnifications can be seen in **Figure S1**. In contrast, all adsorbents prepared from the longer chain monomer, $PEGMA_{950}$, appeared identical to the PDVB precursor (**Figure 3 and 1A**). This cast doubt over the success of the $PEGMA_{950}$ grafting.

352 To determine the success of grafting, PDVB-*g*-PEGMA$_{950}$ (20% PEGMA) was
353 probed using a crude assay to assess surface hydrophilicity. A 10 µL droplet of an
354 aqueous solution of green food dye was pipetted onto the surface of the bulk
355 adsorbents. The PDVB was employed as negative control. As successful grafting of
356 PDVB-*g*-PEGMA$_{360}$ (10% PEGMA) was evident from the SEM assessment, this
357 adsorbent was employed as a positive control. The aqueous dye solution was repelled
358 from the hydrophobic PDVB, beading on the surface. In contrast, the aqueous
359 solution penetrated the PDVB-*g*-PEGMA$_{360}$ wetting the adsorbent (**Figure S2**). As
360 with PDVB-*g*-PEGMA$_{360}$, the aqueous dye solution immediately penetrated the
361 PDVB-*g*-PEGMA$_{950}$, suggesting the successful the grafting of PEGMA$_{950}$.
362
363 To evaluate the extent of protein interactions with each of the SPE adsorbents a
364 qualitative fluorescent assay was employed. As HSA is the most abundant human
365 plasma protein it was selected as the probe. HSA is a 67 kDa globular protein with
366 dimensions of 3.8 nm × 15 nm, therefore any interactions are likely limited to the
367 external surface of the adsorbent. A typical SPE workflow was employed for this
368 assay. The adsorbent bed was conditioned with methanol then equilibrated with water,
369 a 400 µL aliquot of 50 mg L^{-1} HSA labeled with fluorescamine was passed through
370 the adsorbent bed. The adsorbent was flushed with water to remove any residual
371 protein. The intensity of the fluorescent signal of each adsorbent was observed using
372 an optical microscope. The intensity of the fluorescent signal provides a qualitative
373 insight into the extent of protein interactions with the adsorbent; the desired low level
374 of protein interaction is implied by low fluorescence intensity. The background
375 fluorescent signal for each material can be seen in the supplementary information
376 (**Figure S3**).

The PDVB presents a substantial fluorescent signal, despite the small pores preventing HSA from accessing the large internal surface area it appears a considerable amount of HSA has been adsorbed on the external hydrophobic surface (**Figure 4**). A high fluorescent signal was seen for both PDVB-*g*-PEGMA$_{360}$ and PDVB-*g*-PEGMA$_{950}$ that was prepared with 5% PEGMA in the graft solution. This result suggests 5% PEGMA is not sufficient to prevent protein interactions, therefore these adsorbents were not analyzed further. In contrast, increasing the PEGMA concentration to 10% in the graft solution decreased the fluorescent signal. The fluorescent signal observed for PDVB-*g*-PEGMA$_{360}$ was reduced substantially. The signal for PDVB-*g*-PEGMA$_{950}$ was also lessened but to a lower extent. PDVB-*g*-PEGMA$_{950}$ prepared using 20% PEGMA$_{950}$ in the graft solution yielded a much lower fluorescent response compared to PDVB-*g*-PEGMA$_{950}$ prepared using 10% PEGMA$_{950}$. As the grafting of PEGMA$_{950}$ (20%) and PEGMA$_{360}$ (10%) was sufficient to substantially reduce protein binding these adsorbents were further investigated.

To characterize grafting both PDVB-*g*-PEGMA adsorbents were compared to the precursor PDVB using ATR-FTIR. The overlaid FTIR spectra revealed distinct changes in the chemical functionality (**Figure 5**). The spectrum corresponding to PDVB-*g*-PEGMA$_{360}$ exposed a distinct band at 1114 cm^{-1} which can be attributed to ether functionality. The bands at 1724 cm^{-1} and 1247 cm^{-1} can be credited to the ester functionality of the PEGMA monomer. Lastly, the wide band at 3449 cm^{-1} is indicative of the terminal hydroxyl group on the PEGMA$_{360}$ chain. The spectral changes are subtler for the PDVB-*g*-PEGMA$_{950}$, the band at 1114 cm^{-1} (ether functional group) is the dominant change. The relative intensity of this band is

402 expected due to the large number of the repeating glycol units. In contrast, only a very
403 small band is seen at 1724 cm^{-1} relating to the single ester group on each of the
404 attached monomer chains. **Figure 5** infers a higher density of grafting was achieved
405 for the shorter chain length $PEGMA_{360}$.
406
407 The results above are corroborated by solid-state NMR, for ^{13}C CP-MAS NMR, the
408 appearance of the signal at 71 ppm is attributed to the PEG side chain (**Figure 2**) [31].
409 Intrinsically, the ^{13}C CP-MAS NMR analysis is not quantitative as the signal
410 enhancement is biased towards the more rigid components of a sample. Therefore, ^{1}H
411 NMR was employed to quantitate PEGMA grafting, details of the experimental setup
412 can be seen in the supplementary information **Section S5**. The ^{1}H NMR spectrum of
413 PDVB exhibits a signal at 6.7 ppm, a small shoulder at 3.2 ppm is also seen (**Figure**
414 **6**) [23]. Following grafting, both PDVB-*g*-PEGMA adsorbents display a narrower
415 signal for PDVB at 6.7 ppm (insert **Figure 6**), this suggests that the ungrafted PDVB
416 is more rigid than the PDVB-*g*-PEGMA adsorbents (**Figure 6**) [31]. The difficulty to
417 completely dry the PDVB-*g*-PEGMA adsorbents due to the introduction of the
418 hydrophilic coating is the most likely cause for the increased mobility of the PDVB
419 signal in the PDVB-*g*-PEGMA spectra. The strong signal at 3.5 ppm is attributed to
420 the PEG chain, the PEG signal is much narrower than the PDVB signal as the chains
421 have a higher mobility than the crosslinked PDVB monolith (**Figure 6**). The peak
422 areas of the ^{1}H NMR spectra were employed to quantify the PEGMA content of the
423 grafted adsorbents (**Table S3 and S4**). The PEGMA content was quantified in the
424 grafted samples as the mass (*m*) ratio of PEGMA to PDVB using Equations (1).
425

$$\frac{m_{\mathrm{PEGMA}}}{m_{\mathrm{PDVB}}} = \frac{I_{\mathrm{PEG}}}{I_{\mathrm{PDVB}}} \cdot \frac{N_{\mathrm{DVB}}}{N_{\mathrm{PEGMA}}} \cdot \frac{M_{\mathrm{PEGMA}}}{M_{\mathrm{DVB}}} \quad (1)$$

where *I* is the peak area of the monomer units in the NMR spectrum, *N* is the number of protons from which this signal originates and *M* is the molar mass of a monomer unit. Details of the equation derivation and the data processing are given in supporting information (**Section S6**). From this analysis the PEGMA content (% w/w) in the grafted samples was estimated to be 29.9 ± 1.6% for PDVB-*g*-PEGMA$_{360}$ and 7.7 ± 1.2% for PDVB-*g*-PEGMA$_{950}$. This confirms that a higher degree of grafting was seen for the shorter chain length PEGMA$_{360}$. The reason for the lower observed grafting density of PEGMA$_{950}$ was not investigated further but possible reasons may be a lower reactivity of the PEGMA$_{950}$ monomer or a steric hindrance due to the longer glycol chain limiting access to the surface.

The permeability was determined, as outlined above for PDVB, to determine if the grafted PEGMA layer was detrimental to the operation of the miniaturized SPE cartridge. The permeability was estimated to be 1.7 x 10^{-15} m^2 (13% propagated error) and 3.7 x 10^{-15} m^2 (12% propagated error) for PDVB-*g*-PEGMA$_{360}$ and PDVB-*g*-PEGMA$_{950}$ respectively. Unsurprisingly, the permeabilities of the miniaturized SPE cartridges were reduced following the grafting reaction. The PDVB-*g*-PEGMA$_{360}$, with the most obvious grafted layer, demonstrated the greatest decrease in permeability. However, as the digital syringe drive was still able to successfully pass fluid through the miniaturized SPE cartridge at 1 mL min^{-1} the decreased permeability was not considered detrimental to the miniaturized SPE workflow.

Assessment of the adsorbent performance for SPE

Frontal analysis was employed to evaluate the performance of each SPE adsorbent as the shape of the breakthrough curve provides key insight into the adsorbents suitability for SPE. To achieve a complete SPE extraction a rapid an efficient equilibrium between the analyte and the adsorbent (a sharp breakthrough curve) is critical. The presence of the hydrophilic layer must not dramatically impede the interactions between the analyte and the inner hydrophobic surface. If the analyte is unable to achieve a rapid equilibrium with the adsorbent reduced extraction recoveries and high sample carryovers will result. To determine SPE suitability of the adsorbents, PDVB, PDVB-*g*-PEGMA$_{950}$ and PDVB-*g*-PEGMA$_{360}$ were prepared in MEPS cartridges, this format was explored as it could be seamlessly interfaced with HPLC-UV. Anisole (0.32 – 0.42 nm^2) and ibuprofen (0.35 – 0.65 nm^2) in aqueous solutions were employed as probe molecules. The capacity factor (k'), volume of analyte breakthrough (V_B), volume of analyte retention (V_R), the standard deviation of the derivative curve ($2\sigma_v$) and the amount of analyte adsorbed (q_c) were selected as metrics for the evaluation. The void volume (V_0) of the system, including the MEPS cartridge filled with each of the polymer monoliths, was determined using uracil. For all cartridges the V_0 was 80 µL.

The breakthrough curves of both anisole and ibuprofen can be seen in **Figure 7.** The V_B is defined as the volume of sample that has passed through the adsorbent until 1% of the maximum analyte signal is measured at the outlet. V_B can be calculated from **Equation 2,**

$$V_B = V_R - 2\sigma_v \quad (2)$$

where V_R is the retention volume determined from the inflection point of the curve and $2\sigma_v$ is the standard deviation of the derivative curve [32]. Results of anisole

breakthrough for PDVB-*g*-PEGMA$_{950}$ mirrored the shape of the PDVB curve (**Figure 7A**). A small reduction in the V_B was revealed which is consistent with the reduced *k'* (**Table 1**). Further, a small decrease in the sharpness (2 σ_v) of the PDVB-*g*-PEGMA$_{950}$ curve was observed. In contrast, the anisole breakthrough curve for PDVB-*g*-PEGMA$_{360}$ shows a premature V_B, the anisole is detected at the cartridge outlet almost immediately. The shallow breakthrough curve (large 2 σ_v) suggests there is insufficient time for the analyte to penetrate the PEGMA$_{360}$ coating when a flow rate of 500 µL min^{-1} is employed.

Equation 3 was employed to determine the amount of analyte adsorbed (q_c) for each SPE adsorbent.

$$q_c = (t_R - t_0) f C \quad (3)$$

where t_R, is the retention time, t_0 is the void time, f is the flow rate and C is the analyte concentration. **Table 1** lists the q_c for all adsorbents. The amount of analyte adsorbed was reduced slightly following the grafting of the PEGMA$_{950}$ layer. Interestingly, despite the reduced V_B of PDVB-*g*-PEGMA$_{360}$ the q_c of the adsorbent has largely been preserved. However, due the poor analyte diffusion through the PEGMA layer it was determined that this adsorbent is unsuitable for rapid miniaturized SPE workflows and PDVB-*g*-PEGMA$_{360}$ was not investigated further. To broaden the validation, ibuprofen breakthrough curves were compared for PDVB and PDVB-*g*-PEGMA$_{950}$ (**Figure 7B**). As with anisole, a small reduction in the *k'*, V_B, V_R, σ_v and q_c of ibuprofen was observed following the grafting of PEGMA$_{950}$ (**Table 1**). However, the overall shape of the curve was maintained relative to PDVB. The results indicate that the grafted layer of PEGMA$_{950}$ does not dramatically diminish analyte/adsorbent interactions. To support this observation the bulk PDVB-*g*-

PEGMA$_{950}$ was analyzed using argon adsorption/desorption at 77 K (**Figure S5**). The isotherm of the PDVB-*g*-PEGMA$_{950}$ reveals a similar pore structure to PDVB. In addition, the surface area, 495 m^2g^{-1}, was equivalent to the surface area of PDVB confirming that PEGMA$_{950}$ does not drastically alter analyte/adsorbent interactions.

To broaden the validation of biocompatibility the degree of protein binding was quantitated chromatographically. The amount of HSA adsorbed was measured for both the PDVB and the PDVB-*g*-PEGMA$_{950}$ using offline SPE. An aliquot of HSA was passed through the adsorbent bed and any reduction in peak area of the effluent corresponded to non-specific protein binding. The PDVB adsorbed 31 ± 2.41% of the HSA sample. Given that only a very small external surface area is available for interaction the amount of HSA adsorbed was substantial. While not completely eliminated, the amount of HSA adsorbed to the PDVB-*g*-PEGMA$_{950}$ was reduced to 12 ± 0.49%. In future studies, a further increase in the amount of PEGMA$_{950}$ in the graft solution could be investigated to aid the complete elimination of protein binding.

The final performance qualifier of these adsorbents is analyte recovery; which is a critically important performance characteristic of miniaturized SPE. A comparative study of recovery was undertaken to benchmark the performance of the PDVB-*g*-PEGMA$_{950}$ against the PDVB adsorbent. Recovery of 10 mg L^{-1} ibuprofen was determined for the two adsorbents. The PDVB offered an analyte recovery of 92 ± 0.30% compared to 78 ± 0.93% using PDVB-*g*-PEGMA$_{950}$. Reduced analyte recovery was expected given reduction the k' and V_B seen in **Table 1.** Regardless of this reduction, 78% is still considered a high value for analyte recovery. This qualifies the

PDVB-*g*-PEGMA$_{950}$ as a highly suitable biocompatible adsorbent for miniaturized SPE.

Application to a real sample

At-line ESI-MS was employed to finalize the assessment of PDVB-*g*-PEGMA$_{950}$ for a miniaturized SPE clean up of human plasma. By infusing the processed sample directly from the adsorbent bed into the ESI-MS using the at-line approach we can gain an impression of the effectiveness of the sample clean up [27]. A diluted (20% v/v) plasma sample spiked with ibuprofen was processed using both the PDVB and the PDVB-*g*-PEGMA$_{950}$ adsorbents. The extracted ion chromatogram of the elution profiles were compared between the PDVB and the PDVB-*g*-PEGMA$_{950}$ (**Figure 8**). To this end, the peak area of the ibuprofen elution profile from the PDVB-*g*-PEGMA$_{950}$ was 30 % greater than the profile obtained using hydrophobic PDVB. Here we see that the PDVB assay was crippled by the hydrophobic surface chemistry, the adsorbed protein matrix contaminants led to a dramatic reduction in assay sensitivity. The biocompatibility of the PDVB-*g*-PEGMA$_{950}$ adsorbent has been clearly demonstrated for the fast and efficient purification of analytes in highly complex biological samples.

Conclusions

The inherent pore structure of PDVB makes it highly appealing for a size selective miniaturized SPE. Despite the desirable pore structure of PDVB, use with highly complex biological samples rich in proteins can be problematic due to the non-specific protein adsorption to the hydrophobic surface. PEGMA$_{360}$ and PEGMA$_{950}$ were grafted to the RVGs of the PDVB to provide biocompatible adsorbents. The

546 grafted layer was carefully characterized for both PDVB-*g*-$PEGMA_{360}$ and PDVB-*g*-
547 $PEGMA_{950}$. The thick coating of PDVB-*g*-$PEGMA_{360}$ was a double-edged sword,
548 while the coating prevented proteins from accessing the hydrophobic surface,
549 substantial time was required for the analyte to interact with the adsorbent thus
550 diminishing the adsorbents suitability for miniaturized SPE. The grafted $PEGMA_{950}$
551 did not dramatically affect the SPE adsorptive properties. The PDVB-*g*-$PEGMA_{950}$
552 revealed only a small reduction in the amount of analyte loaded on the adsorbent bed.
553 Furthermore, protein adsorption was substantially restricted by the grafted
554 $PEGMA_{950}$. The PDVB-*g*-$PEGMA_{950}$ adsorbent was demonstrated to produce cleaner
555 extracts for a more sensitive ESI-MS assay. The superiority of the PDVB-*g*-
556 $PEGMA_{950}$ adsorbent is extremely beneficial for the rapid and efficient miniaturized
557 SPE purification of analytes in protein rich biological samples.
558
559 **Acknowledgments**
560 RAS is the recipient of an Australian Research Council Australian Research
561 Fellowship (DP110104923). EC is the recipient of an Australian Postgraduate Award.
562 Support from the University of Tasmania Central Science Laboratory is gratefully
563 acknowledged. We gratefully acknowledge Dr. Karsten Gömann and Dr. Sandrin Feig
564 (University of Tasmania) for assistance with scanning electron microscopy and
565 Patrice Castignolles (University of Western Sydney) for helpful discussions.
566
567 **References**
568 1. Westerlund D (1987) D. Chromatographia 24:155–164.

569 2. Annesley TM (2003). Clin Chem 49:1041–1044.

570 3. Chen Y, Guo Z, Wang X, Qiu C (2008). J Chromatogr A 1184:191–219.

571 4. Li Y, Lee ML (2009). J Sep Sci 32:3369–3378.

572 5. Georgi K, Boos KS (2004). LC GC Eur 17:21–24.

573 6. Cassiano NM, Lima VV, Oliveira RV, de Pietro AC, Cass QB (2006). Anal
574 Bioanal Chem 384:1462–1469.

575 7. Souverain S, Rudaz S, Veuthey J-L (2004). J Chromatogr B 801:141–156.

576 8. Hagestam IH, Pinkerton TC (1985). Anal Chem 57:1757–1763.

577 9. Cook SE, Pinkerton TC (1986). J Chromatogr A 368:233–248.

578 10. Turson M, Zhou M, Jiang P, Dong X (2011). J Sep Sci 34:127–134.

579 11. Candish E, Wirth H-J, Gooley AA, Shellie RA, Hilder EF (2015). J
580 Chromatogr A 1410:9–18.

581 12. Yang H, Ulbricht M (2008). Macromol Mater Eng 293:419–427.

582 13. Gisch DJ, Hunter BT, Feibush B (1988). J Chromatogr A 433:264–268.

583 14. Kanda T, Shirota O, Ohtsu Y, Yamaguchi M (1996). J Chromatogr A 722:115–
584 121.

585 15. Buchmeiser MR (2007). Polymer 48:2187–2198.

586 16. Smirnov KN, Dyatchkov IA, Telnov MV, Pirogov AV, Shpigun OA (2011). J
587 Chromatogr A 1218:5010–5019.

588 17. Gu B, Armenta JM, Lee ML (2005). J Chromatogr A 1079:382–391.

589 18. Krenkova J, Lacher NA, Svec F (2009). Anal Chem 81:2004–2012.

590 19. Barlow KJ, Hao X, Hughes TC, Hutt OE, Polyzos A, Turner KA, Moad G
591 (2014). Polym Chem 5:722–732.

592 20. Peters EC, Svec F, Fréchet JMJ, Viklund C, Irgum K (1999). Macromolecules
593 32:6377–6379.

594 21. Hubbard KL, Finch JA, Darling GD (1999). React Funct Polym 42:279–289.

595 22. Tripp JA, Needham TP, Ripp EM, Konzman BG, Homnick PJ (2010) Reactive
596 & Functional Polymers. React Funct Polym 70:414–418.

597 23. Gaborieau M, Nebhani L, Graf R, Barner L, Barner-Kowollik C (2010).
598 Macromolecules 43:3868–3875.

599 24. Claridge TDW (2009) High-Resolution NMR Techniques in Organic
600 Chemistry, Second Edition.

601 25. Morcombe CR, Zilm KW (2003). J Magn Reson 162:479–486.

602 26. Sýkora D, Peters EC, Svec F (2000). Macromol Mater Eng 275:42–47.

603 27. Candish E, Gooley A, Wirth H-J, Dawes PA, Shellie RA, Hilder EF (2012). J
604 Sep Sci 35:2399–2406.

605 28. Jarmalavičienė R, Kornyšova O, Westerlund D, Maruška A (2003). Anal
606 Bioanal Chem 377:902–908.

607 29. Jarmalavičienė R, Kornyšova O, Bendokas V, Westerlund D, Buszewski B,
608 Maruška A (2008). Anal Bioanal Chem 391:2323–2328.

609 30. D'Sa RA, Meenan BJ (2010). Langmuir 26:1894–1903.

610 31. Mangiante G, Alcouffe P, Burdin B, Gaborieau M, Zeno E, Petit-Conil M,
611 Bernard J, Charlot A, Fleury E (2013). Biomacromolecules 14:254–263.

612 32. Bielicka-Daszkiewicz K, Voelkel A (2009). Talanta 80:614–621.

613

614 **Table 1.** Capacity factor, breakthrough volume, retention volume, standard deviation
615 of the derivative curve and amount of analyte adsorbed for PDVB, PDVB-*g*-PEGMA$_{950}$
616 and PDVB-*g*-PEGMA$_{360}$

Adsorbent	k'	V_B (mL)	V_R (mL)	$2\sigma_v$ (mL)	q_c (mg g^{-1})
Anisole					
PDVB	39	2.8	3.1	0.7	129
PDVB-*g*-PEGMA$_{950}$	35	2.3	2.8	0.8	116
PDVB-*g*-PEGMA$_{360}$	34	0.5	2.6	1.6	106
Ibuprofen					
PDVB	122	7.8	9.6	2.6	43
PDVB-*g*-PEGMA$_{360}$	118	7.2	9.8	2.7	38

617
618
619

Figure 1. The dry state characterization of PDVB. A) SEM images, top 2000× magnification and bottom 20 000× magnification. B) The argon adsorption (■) and desorption (o) isotherms at 77 K and C) corresponding pore size data determined by NLDFT.

Figure 2. Solid-state ^{13}C CP-MAS NMR spectra of all adsorbents. Bottom) PDVB, Middle) The PDVB-*g*-PEGMA$_{950}$, Top) PDVB-*g*-PEGMA$_{360}$. The chemical shifts are assigned in Scheme 1.

Figure 3. SEM images of the surface of PDVB-*g*-PEGMA$_{360}$ and PDVB-*g*-PEGMA$_{950}$ prepared from 5, 10 and 20% PEGMA in the graft solution. The magnification of all images is 10 000× and the scale bar corresponds to 5 μm.

Figure 4. Optical microscopy images of protein interactions for the developed adsorbents, fluorescently labeled HSA was flushed through the PDVB scaffold as well the grafted PDVB adsorbents with increasing percentages of PEGMA$_{950}$ and PEGMA$_{360}$.

Figure 5. ATR-FTIR spectra of PDVB, PDVB-*g*-PEGMA$_{950}$ and PDVB-*g*-PEGMA$_{360}$.

Figure 6. Solid-state ^{1}H MAS NMR spectra of all adsorbents. A) PDVB, B) PDVB-*g*-PEGMA$_{950}$, C) PDVB-*g*-PEGMA$_{360}$.

Figure 7. A) Anisole breakthrough for PDVB (---),PDVB-*g*-PEGMA$_{950}$ (—) and PDVB-*g*-PEGMA$_{360}$ (- -). B) Ibuprofen breakthrough for PDVB (---) and PDVB-*g*-PEGMA$_{950}$ (—).

Figure 8. Comparison of sample clean up and at-line MS elution profiles of ibuprofen in a dilute plasma sample (20% v/v) using PDVB and PDVB-*g*-PEGMA$_{950}$ adsorbents

Figure 1

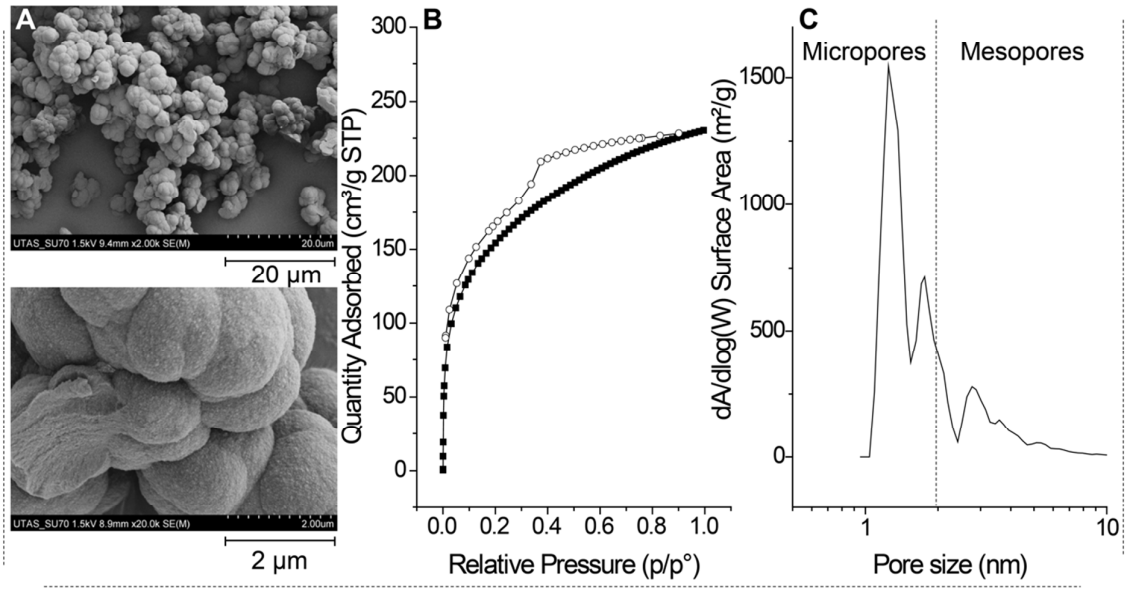
A
UTAS_SU70 1.5kV 9.4mm x2.00k SE(M)
20.0um
20 µm
UTAS_SU70 1.5kV 8.9mm x20.0k SE(M)
2.00um
2 µm
B
Quantity Adsorbed (cm³/g STP)
300
250
200
150
100
50
0
0.0
0.2
0.4
0.6
0.8
1.0
Relative Pressure (p/p°)
C
Micropores
Mesopores
dA/dlog(W) Surface Area (m²/g)
1500
1000
500
0
1
10
Pore size (nm)

Figure 2

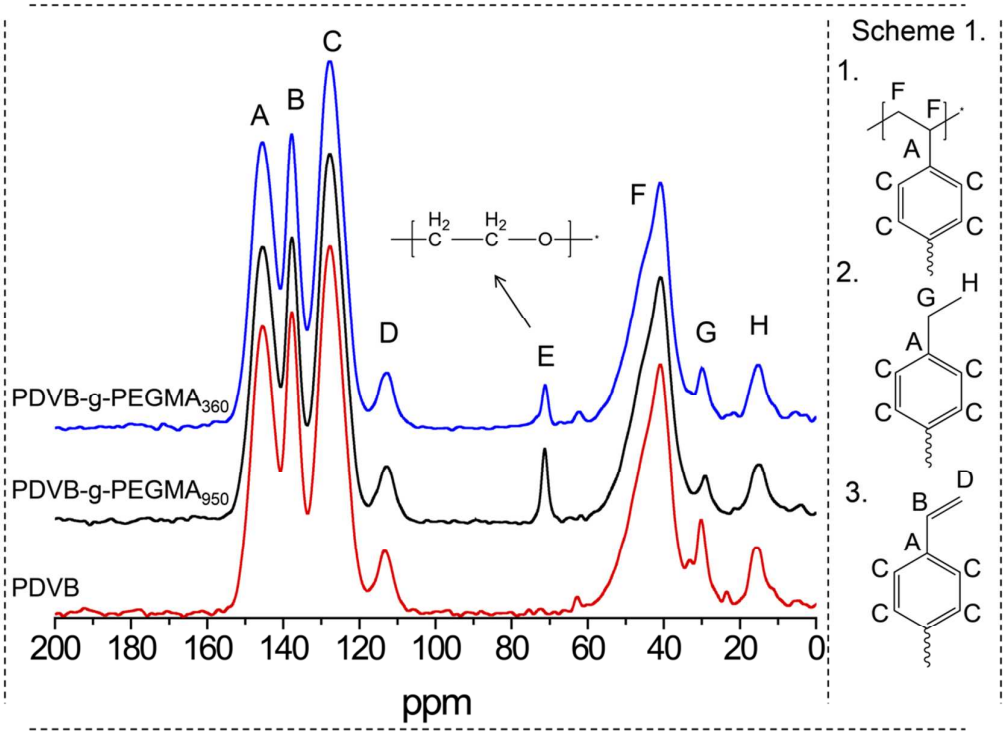
A
B
C
D
E
F
G
H
PDVB-g-PEGMA360
PDVB-g-PEGMA950
PDVB
200 180 160 140 120 100 80 60 40 20 0
ppm
Scheme 1.
1.
2.
3.

Figure 3

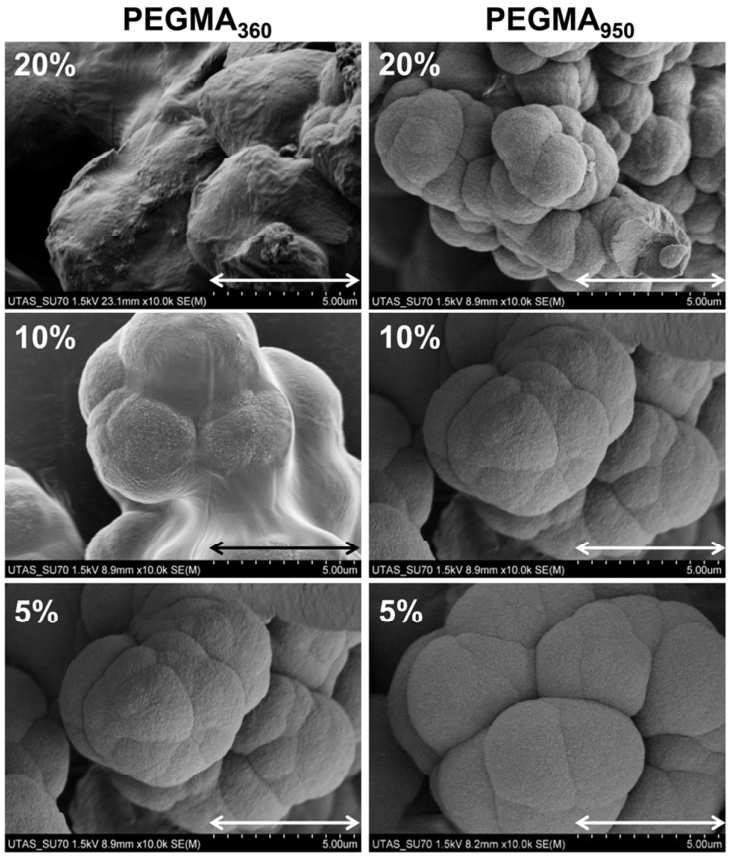
PEGMA360
PEGMA950
20%
20%
10%
10%
5%
5%
UTAS_SU70 1.5kV 23.1mm x10.0k SE(M)
UTAS_SU70 1.5kV 8.9mm x10.0k SE(M)
UTAS_SU70 1.5kV 8.9mm x10.0k SE(M)
UTAS_SU70 1.5kV 8.9mm x10.0k SE(M)
UTAS_SU70 1.5kV 8.2mm x10.0k SE(M)
5.00um

Figure 4

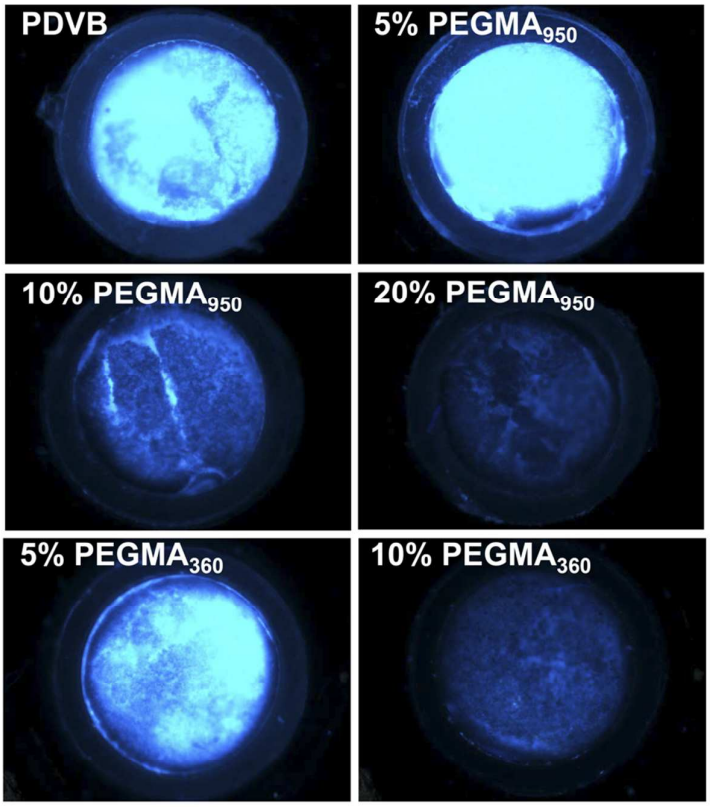
PDVB
5% PEGMA950
10% PEGMA950
20% PEGMA950
5% PEGMA360
10% PEGMA360

Figure 5

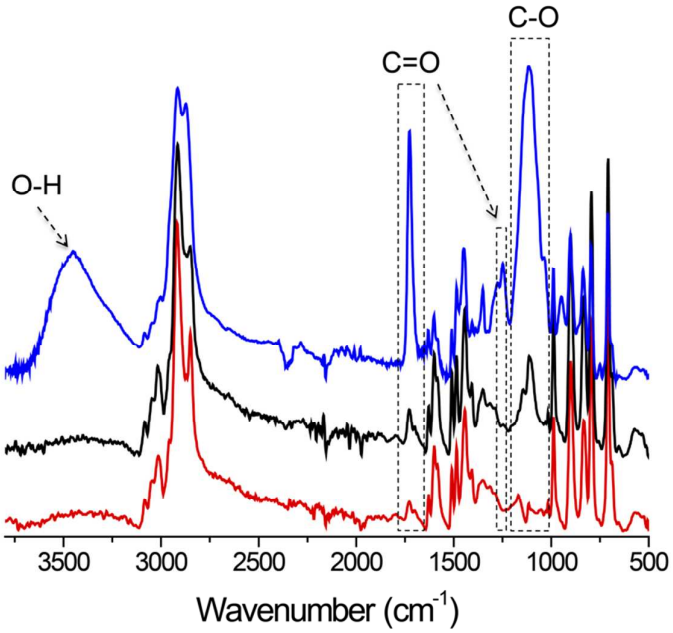

Figure 6

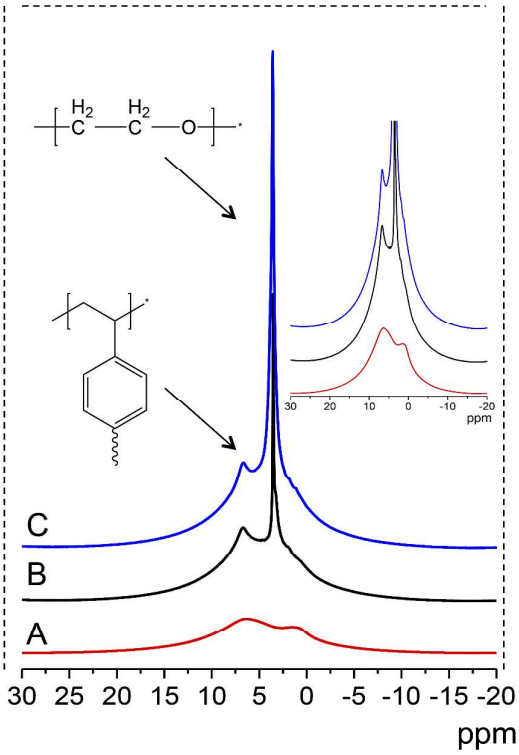

Figure 7

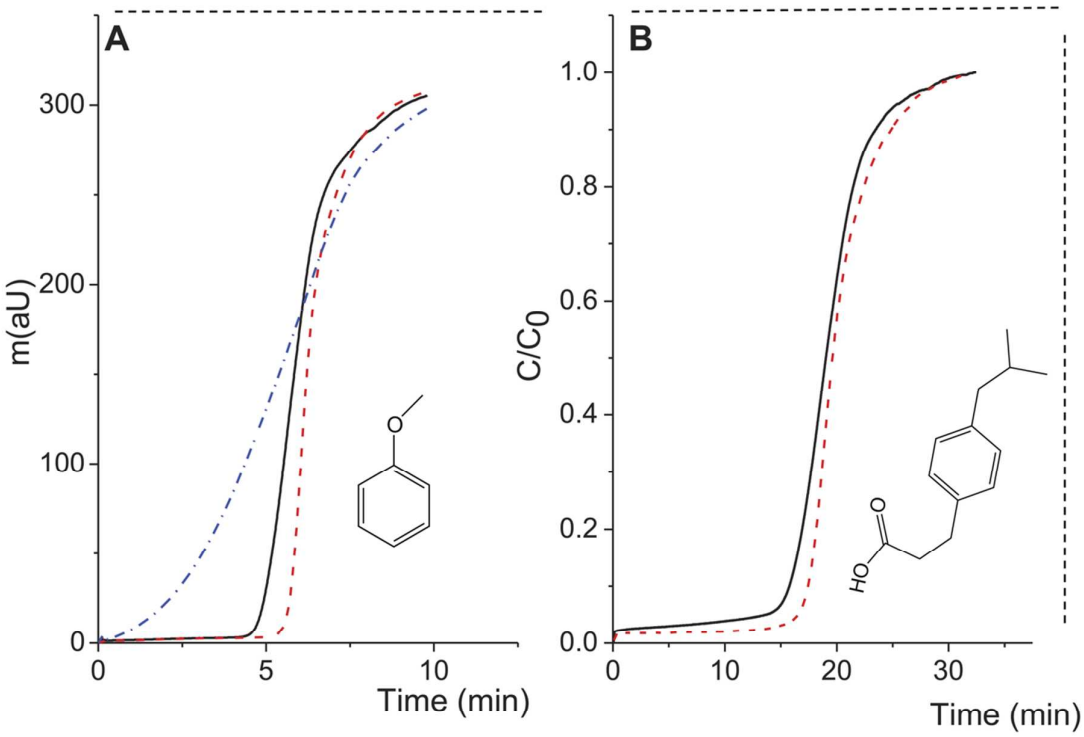
A
300
200
100
0
m(aU)
0
5
10
Time (min)
B
1.0
0.8
0.6
0.4
0.2
0.0
C/C0
HO
O
0
10
20
30
Time (min)

Figure 8

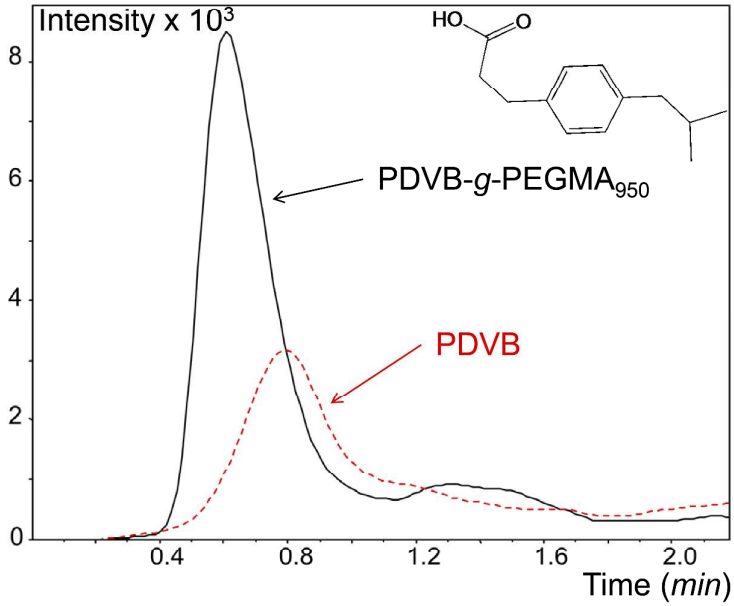
Intensity x 10^3
8
6
4
2
0
0.4
0.8
1.2
1.6
2.0
Time (min)
HO
O
PDVB-g-PEGMA950
PDVB

Analytical and Bioanalytical Chemistry

Electronic Supplementary Material

Poly(ethylene glycol) functionalization of monolithic poly(divinyl benzene) for improved miniaturized solid phase extraction of protein-rich samples

Esme Candish, Aminreza Khodabandeh, Marianne Gaborieau, Thomas Rodemann, Robert A. Shellie, Andrew A. Gooley, Emily F. Hilder

Section S1 ^{13}C CP-MAS NMR

Table S1 Complete ^{13}C chemical shift assignment for ^{13}C NMR spectra of PDVB, PDVB-g-PEGMA$_{950}$ and PDVB-g-PEGMA$_{360}$ (seen in Fig. 2)

Group	Chemical shift (ppm)	Assignment
A	145	aromatic ring (adjacent to ethyl or backbone)
B	138	aromatic ring
C	128	PDVB benzene ring
D	113	C=C (C not adjacent to aromatic ring)
E	71	CH_2-CH_2-O- of PEG side chain
	63	residual porogen 1-dodecanol
F	41-50	CH back bone of PDVB and poly methacrylate backbone of PEGMA
		CH_2 back bone of PDVB and poly methacrylate backbone of PEGMA
	30	residual porogen 1-dodecanol
G	30	CH_2 of ethyl on aromatic ring
	23	residual porogen 1-dodecanol
H	16	CH_3 of ethyl on aromatic ring

Note: There are three types of structural aromatics present in the PDVB monoliths (prepared from 80% DVB) 1) both the vinyl groups have reacted to form the crosslinked monolith, 2) the uncrosslinked ethylvinyl benzenes, 3) the DVB unit where only one of the vinyl groups has reacted leaving a residual vinyl groups (RVG).

Section S2 SEM analysis of the PDVB, PDVB-g-$PEGMA_{360}$ (10%) and PDVB-g-$PEGMA_{950}$ at increasing magnification

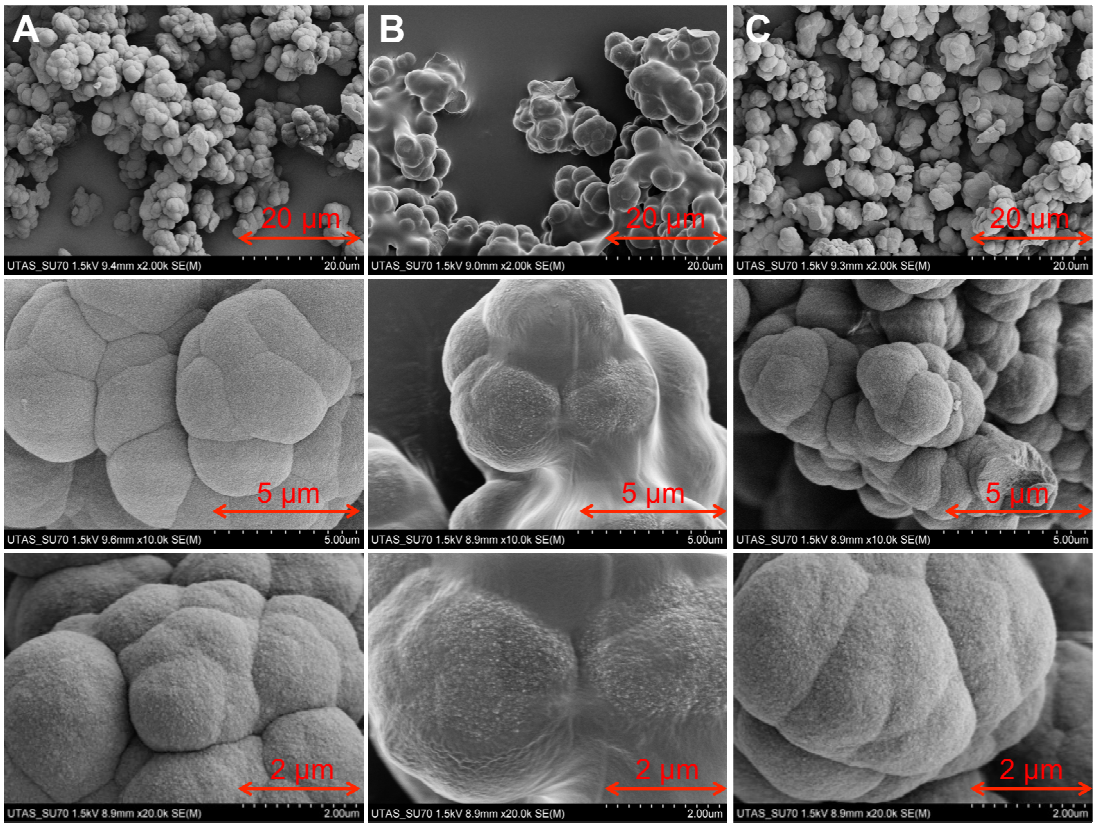

Fig. S1 SEM images of (A) PDVB, (B) PDVB-g-$PEGMA_{360}$ (10%) and (C) PDVB-g-$PEGMA_{950}$ (20%). The magnification in the top is 2000x, middle is 10 000x and bottom is 20 0000x

Section S3 Crude analysis of surface hydrophilicity with aqueous solutions

Fig. S2 An aqueous solution of green food dye spotted onto PDVB, PDVB-g-$PEGMA_{360}$ and PDVB-g-$PEGMA_{950}$ as an estimate of surface grafting

Section S4 Fluorescence analysis of protein adsorption (blanks)

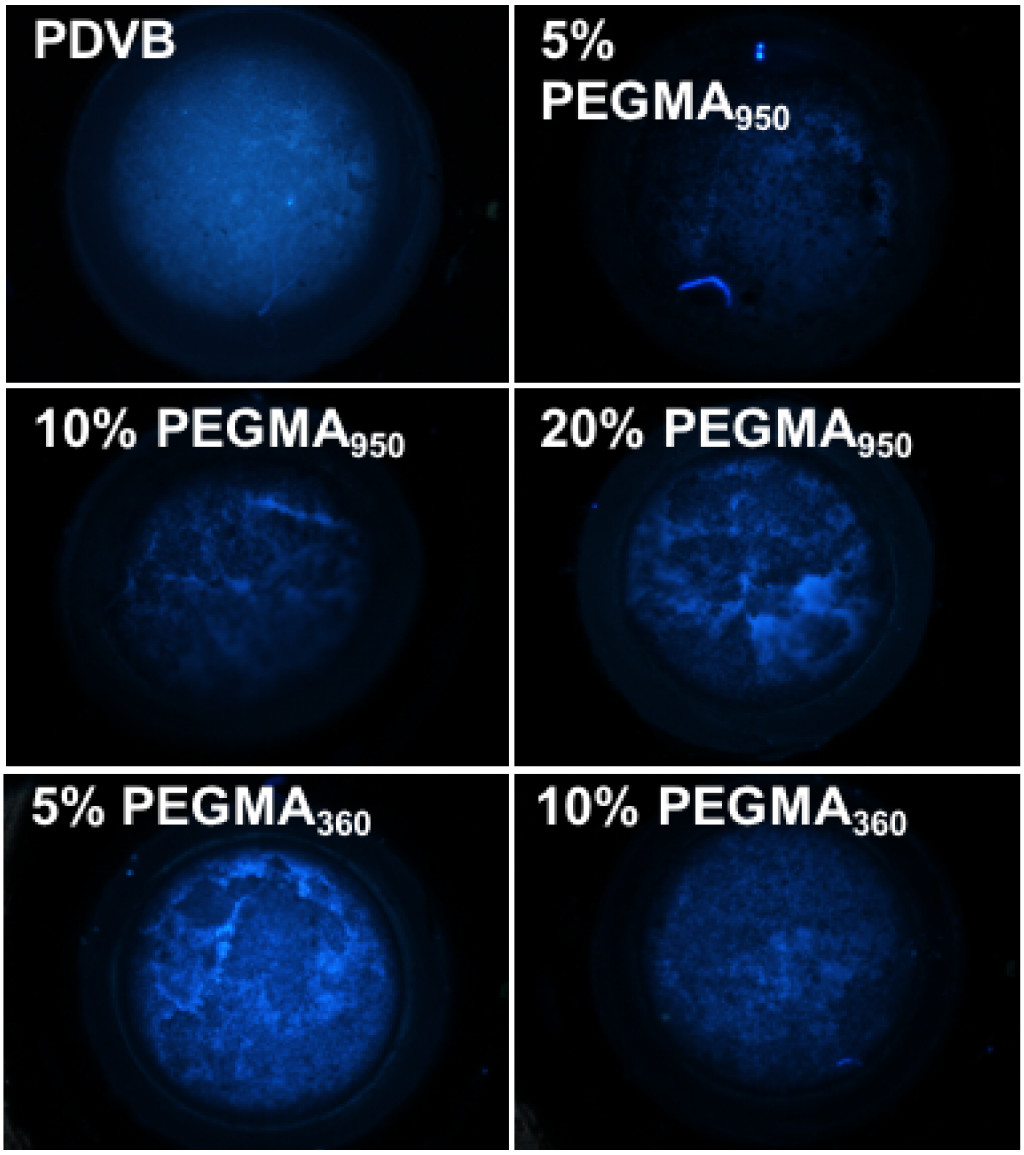

Fig. S3 Optical microscopy images of the background fluorescence for each adsorbent used in the protein binding (fluorescently labelled) assay

Prior to imaging each adsorbent was prepared by flushing the adsorbent bed with 250 µL methanol then with 250 µL water using a flow rate of 50 µL min^{-1}.

Section S5 ATR-FTIR experiments

Table S2 Spectral peak assignment for PDVB, PDVB-g-$PEGMA_{950}$ and PDVB-g-$PEGMA_{360}$ (seen in **Figure 5**)

Wavelength (cm^{-1})	**Assignment**
3449	PEGMA terminal hydroxyl (-OH)
2917, 2873	methyl group (CH_3)
1724, 1247	PEGMA ester (O=C-OR)
1628, 1406, 1015, 987	residual vinyl groups (C=C)
1600,	C-C stretching
1509	para-disubstituted phenyl ring
1484, 1016, 707	monosubstituted phenyl ring
1444	$C=CH_2$, and ring C-H
1114	PEGMA ether
905	mixed assigment: vinyl group, monosubstituted phenyl ring, disubstituted phenyl ringC
832	mixed assignment: monosubstituted phenyl ring, para-disubstituted phenyl ring
793	meta-disubstituted phenyl ring
707	monosubstituted phenyl ring

Hubbard, KL., Finch, JA, Darling, GD. (1998). React Funct Polym, 36, 1–16.

Section S6 ^{1}H NMR experimental set up

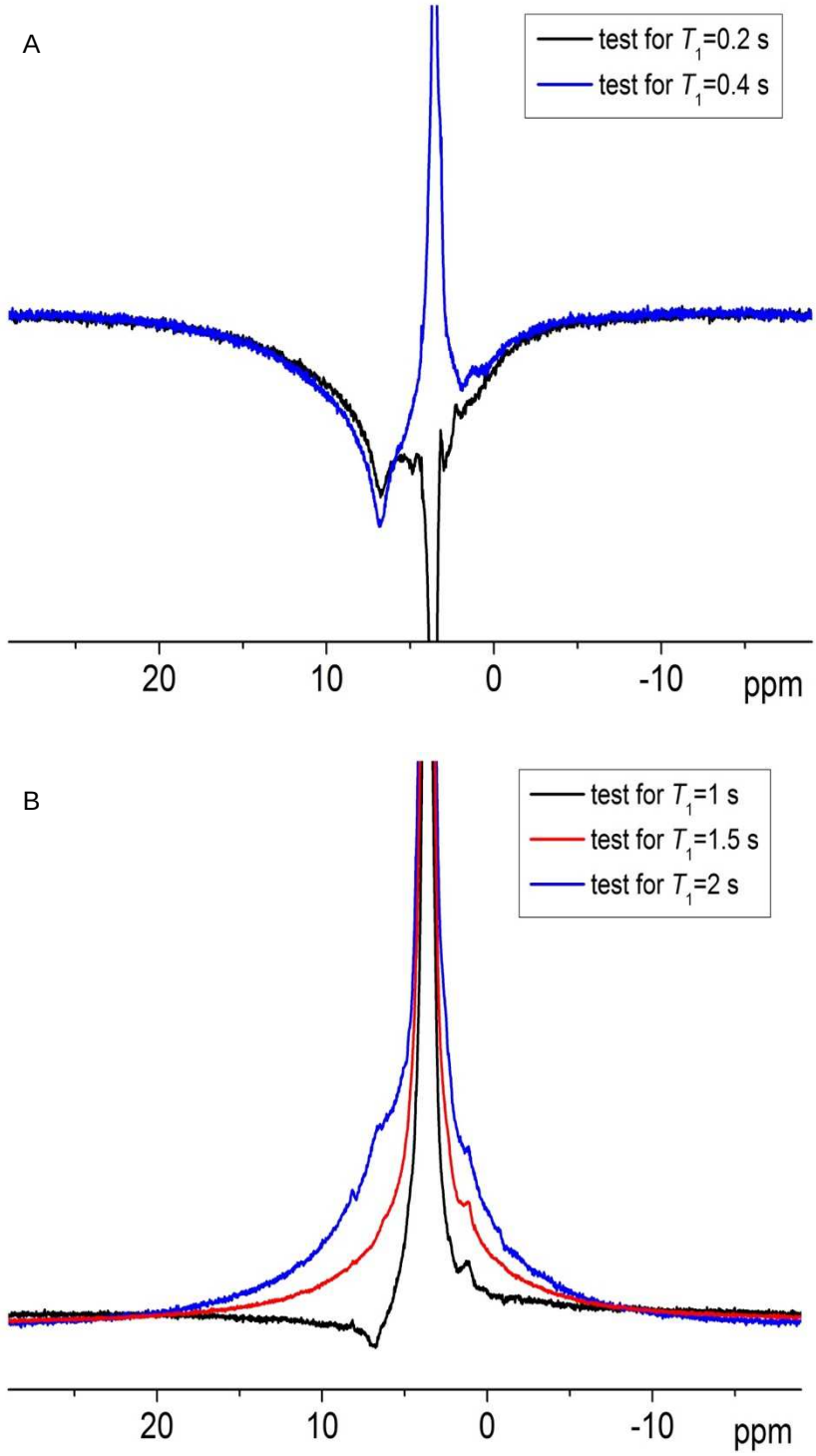

Fig. S4 The one-dimensional inversion-recovery T_1 relaxation measurements of PDVB-g-PEGMA$_{360}$ to assess the relaxation of A) the PEG component at 3.5 ppm and B) the PDVB components at 6.7 ppm

Care was taken to ensure that the magnetization was fully recovered between pulses for ^{1}H NMR signals of both PDVB and PEGMA, in order to determine the true relative signal integrals. To ensure full magnetization recovery between pulses, ^{1}H NMR spectra must be recorded with a delay between pulses longer than 5 times the longitudinal relaxation time (T_1) for each signal of interest. One-dimensional inversion-recovery T_1 relaxation measurements (1D T_1) were conducted, each with a single delay in the "indirect dimension", for delays ranging from 0.1389 to 1.389 s, and corresponding delays between pulses of 5 × 1.44 times that value (0.2 to 2 s).

Phasing the spectra was completed using the same approach as a conventional ^{1}H spectrum. Each signal is negative for short delay values and positive for long delay values, with a zero crossing occurring at T_1 /1.44. The PEG signals at 3.5 ppm exhibited T_1 values between 0.3 and 0.4 s (Fig. S4A), while the PDVB signals exhibited T_1 values between 1 and 2 s, very close to 1.5 s (Fig. S4B). Recording all subsequent ^{1}H NMR spectra experiments with a delay between pulses longer than 5 × 2 = 10 s ensured that full magnetization recovery took place and the ^{1}H NMR spectra were quantitative.

Section S7 Approach to calculate proportionality of PEGMA content in the grafted PDVB samples

The PEGMA content could be quantified in the grafted samples in three ways: first, as the mass ratio of PEGMA to PDVB, second as the molar ratio of PEGMA monomer units to DVB monomer units, and finally as the molar ratio of ethylene glycol monomer units to DVB monomer units. Equations (1) to (3) were employed respectively:

$$\frac{m_{\mathrm{PEGMA}}}{m_{\mathrm{PDVB}}} = \frac{I_{\mathrm{PEG}}}{I_{\mathrm{PDVB}}} \cdot \frac{N_{\mathrm{DVB}}}{N_{\mathrm{PEGMA}}} \cdot \frac{M_{\mathrm{PEGMA}}}{M_{\mathrm{DVB}}} \quad (1)$$

$$\frac{n_{\mathrm{PEGMA}}}{n_{\mathrm{DVB}}} = \frac{I_{\mathrm{PEG}}}{I_{\mathrm{PDVB}}} \cdot \frac{N_{\mathrm{DVB}}}{N_{\mathrm{PEGMA}}} \quad (2)$$

$$\frac{n_{\mathrm{EG}}}{n_{\mathrm{DVB}}} = \frac{I_{\mathrm{PEG}}}{I_{\mathrm{PDVB}}} \cdot \frac{N_{\mathrm{DVB}}}{N_{\mathrm{PEGMA}}} \cdot X_{\mathrm{EG/PEGMA}} \quad (3)$$

where *I* is the peak area of the signal of a monomer unit on the NMR spectrum, *N* is the number of protons from which this signal originates in the monomer unit, *N* is the molar mass of a monomer unit, and $X_{EG/PEGMA}$ is the number of EG monomer units per PEGMA monomer unit.

Derivation of PEGMA to PVB ratios

The peak area (*I)* of a signal of a monomer unit on the NMR spectrum is proportional to the number of protons (*N)* from which this signal originates and to the amount (*n* in mol) of these monomer units. Let *k* be the proportionality constant in a given spectrum:

$$I_{\mathrm{PDVB}} = k \cdot N_{\mathrm{DVB}} \cdot n_{\mathrm{DVB}} \quad (4)$$

$$I_{\mathrm{PEG}} = k \cdot N_{\mathrm{PEGMA}} \cdot n_{\mathrm{PEGMA}} \quad (5)$$

$$I_{\mathrm{total}} = I_{\mathrm{PDVB}} + I_{\mathrm{PEG}} \quad (6)$$

Using the relationship between the *n*, the molar mass (*M)* and the mass (*m)*:

$$I_{\mathrm{PDVB}} = k \cdot N_{\mathrm{DVB}} \cdot \frac{m_{\mathrm{PDVB}}}{M_{\mathrm{DVB}}} \tag{7}$$

$$I_{\mathrm{PEG}} = k \cdot N_{\mathrm{PEGMA}} \cdot \frac{m_{\mathrm{PEGMA}}}{M_{\mathrm{PEGMA}}} \tag{8}$$

The mass ratio of PEGMA and DVB monomer units can be obtained by combination of equations (7) and (8):

$$\frac{m_{\mathrm{PEGMA}}}{m_{\mathrm{PDVB}}} = \frac{I_{\mathrm{PEG}}}{I_{\mathrm{PDVB}}} \cdot \frac{N_{\mathrm{DVB}}}{N_{\mathrm{PEGMA}}} \cdot \frac{M_{\mathrm{PEGMA}}}{M_{\mathrm{DVB}}} \tag{9}$$

$$\frac{m_{\mathrm{PEGMA}}}{m_{\mathrm{PDVB}}} = \frac{I_{\mathrm{PEG}}}{(I_{\mathrm{total}} - I_{\mathrm{PEG}})} \cdot \frac{N_{\mathrm{DVB}}}{N_{\mathrm{PEGMA}}} \cdot \frac{M_{\mathrm{PEGMA}}}{M_{\mathrm{DVB}}} \tag{10}$$

The molar ratio of PEGMA and DVB monomer units can be obtained by combination of equations (4) and (5):

$$\frac{n_{\mathrm{PEGMA}}}{n_{\mathrm{DVB}}} = \frac{I_{\mathrm{PEG}}}{I_{\mathrm{PDVB}}} \cdot \frac{N_{\mathrm{DVB}}}{N_{\mathrm{PEGMA}}} \tag{11}$$

$$\frac{n_{\mathrm{PEGMA}}}{n_{\mathrm{DVB}}} = \frac{I_{\mathrm{PEG}}}{(I_{\mathrm{total}} - I_{\mathrm{PEG}})} \cdot \frac{N_{\mathrm{DVB}}}{N_{\mathrm{PEGMA}}} \tag{12}$$

This ratio can be converted to a molar ratio of ethylene glycol (EG) and DVB monomer units through the number $X_{\mathrm{EG/PEGMA}}$ of EG monomer unit per PEGMA monomer unit:

$$\frac{n_{\mathrm{EG}}}{n_{\mathrm{DVB}}} = \frac{I_{\mathrm{PEG}}}{I_{\mathrm{PDVB}}} \cdot \frac{N_{\mathrm{DVB}}}{N_{\mathrm{PEGMA}}} \cdot X_{\mathrm{EG/PEGMA}} \tag{13}$$

$$\frac{n_{\mathrm{EG}}}{n_{\mathrm{DVB}}} = \frac{I_{\mathrm{PEG}}}{(I_{\mathrm{total}} - I_{\mathrm{PEG}})} \cdot \frac{N_{\mathrm{DVB}}}{N_{\mathrm{PEGMA}}} \cdot X_{\mathrm{EG/PEGMA}} \tag{14}$$

Table S3 Constants needed for the calculations

Name	**Value**	**Unit**
N_{DVB}	10	^{1}H nuclei per monomer unit
N_{PEGMA} for $\mathrm{PEGMA_{360}}$	24.9[a]	^{1}H nuclei per monomer unit
N_{PEGMA} for $\mathrm{PEGMA_{950}}$	77.2[b]	^{1}H nuclei per monomer unit
M_{DVB}	130.19	g·mol^{-1}
M_{PEGMA} for $\mathrm{PEGMA_{360}}$	360	g·mol^{-1} (note: this is M_{n})
M_{PEGMA} for $\mathrm{PEGMA_{950}}$	950	g·mol^{-1} (note: this is M_{n})
$X_{\mathrm{EG/PEGMA}}$ for $\mathrm{PEGMA_{360}}$	6.22[a]	EG monomer units in a PEGMA unit
$X_{\mathrm{EG/PEGMA}}$ for $\mathrm{PEGMA_{950}}$	19.3[b]	EG monomer units in a PEGMA unit

[a] $PEGMA_{360}$ has an -OH end group therefore its molar mass is one methacrylic acid (86.09 $g \cdot mol^{-1}$) and a multiple of the ethylene glycol units (44.05 $g \cdot mol^{-1}$). The average number of ethylene glycol units is thus (360 g mol^{-1} - 86.09 g mol^{-1})/44.05 g mol^{-1} = 6.22.

[b] $PEGMA_{950}$ has a $-CH_3$ end group therefore its molar mass is one methyl methacrylate (100.12 $g \cdot mol^{-1}$) and a multiple of the ethylene glycol units (44.05 $g \cdot mol^{-1}$). The average number of ethylene glycol units is thus (950 $g \cdot mol^{-1}$ - 100.12 $g \cdot mol^{-1}$)/44.05 $g \cdot mol^{-1}$ = 19.3.

The peak area of the PEG signal was estimated by integrating the PEG signal at 3.5 ppm. The integration of the PEG signal is complicated by two situations, first a small component of the PDVB backbone overlaps with the base of the PEG signal. Second the PDVB signal for the ungrafted material is lower than the PDVB for the grafted adsorbents. As an approximate, the peak area of the PEG signal could either be underestimated by setting the baseline above the maximum of the PDVB signal or overestimated by setting the baseline at the level of the valley between this PDVB signal and the PEG signal. The peak area of the PDVB signal was determined as the difference between the total signal integral and the PEG signal integrals.

Table S4 Integrals from NMR spectra

Adsorbent	I_{total}	I_{PEG} ***(underestimate)***	I_{PEG} ***(overestimate)***	I_{PEG}
PDVB-*g*-$PEGMA_{360}$	2782.33	558.27	620.44	589 ± 31
PDVB-*g*-$PEGMA_{950}$	1915.61	120.80	166.98	144 ± 23

Table S5 The ratios of DVB to PEGMA for PDVB-g-PEGMA$_{950}$ and PDVB-g-PEGMA$_{360}$ determined as a mass ratio, a molar ratio of PEGMA to DVB as well as a ratio of EG units to DVB units

Adsorbent	$\frac{m_{PEGMA}}{m_{PDVB}}$ **(wt%)**	$\frac{n_{PEGMA}}{n_{DVB}}$ **(mol%)**	$\frac{n_{EG}}{n_{DVB}}$ **(mol%)**
PDVB-*g*-PEGMA$_{360}$	29.9 ± 1.6	10.80 ± 0.57	67.2 ± 3.5
PDVB-*g*-PEGMA$_{950}$	7.7 ± 1.2	1.05 ± 0.17	20.3 ± 3.3

Section S8 The BET isotherm of PVB-g-PEGMA$_{950}$

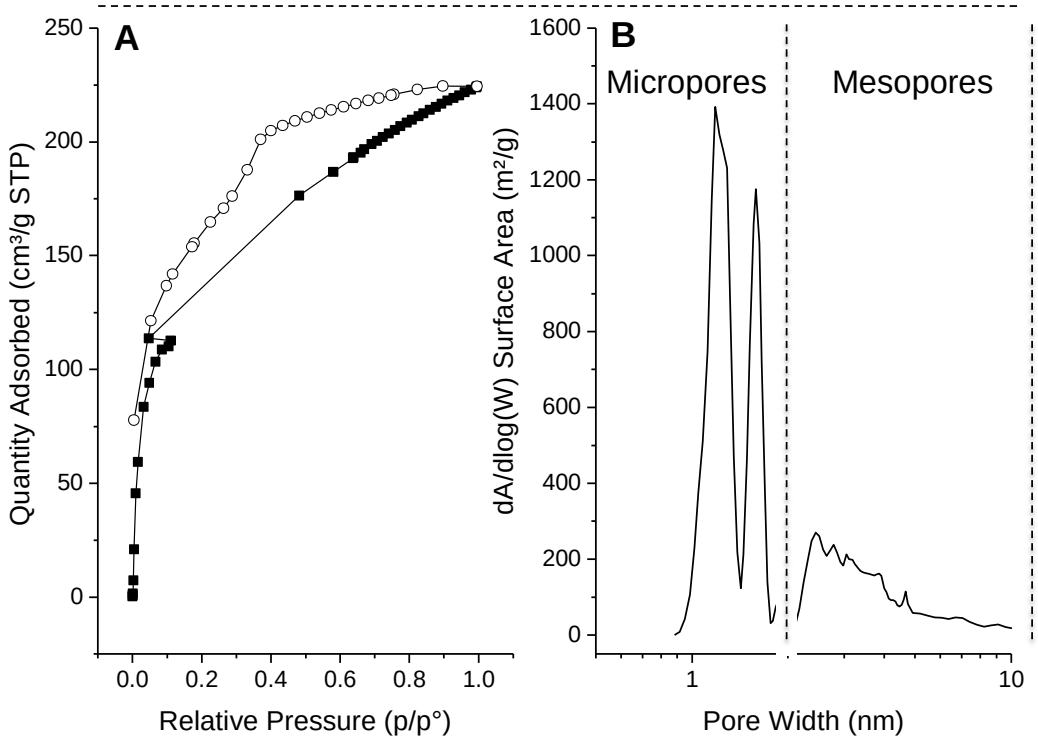

Fig. S5 The argon adsorption (■) and desorption (o) isotherms at 77 K and resulting pore size data determined by NLDFT for PVB-g-PEGMA$_{950}$

Section S9 HPLC-UV chromatograms of protein adsorption and analyte recovery for both PDVB and PDVB-g-PEGMA$_{950}$

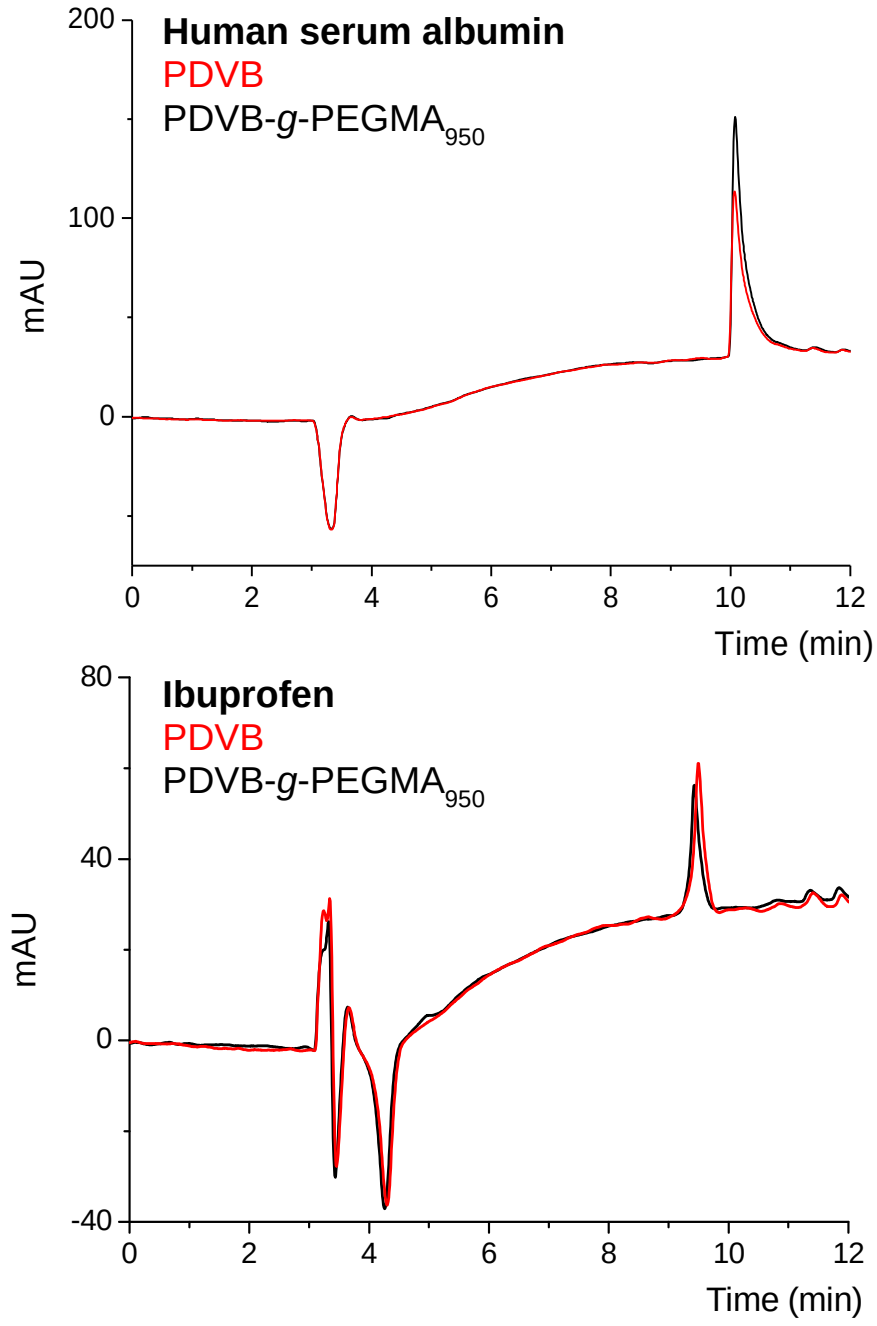

Fig. S6 Top) Human serum albumin recovery for PDVB (red) and PDVB-g-PEGMA$_{950}$ (black). Bottom) Ibuprofen recovery PDVB (red) and PDVB-g-PEGMA$_{950}$ (black)

Section S10 Fabrication repeatability for PDVB and PDVB-g-PEGMA$_{950}$

To determine repeatability of the PDVB fabrication approach the dry state surface area and anisole retention volume (V_B) was measured for three different batches.

Table S6 The surface area of PDVB fabricated for three different batches

Batch	**Surface area (m^2g^{-1})**
1	497
2	487
3	491
Average	**492**
RSD	**1%**

Table S7 Anisole retention volume (V_R) for three different batches of PDVB

Batch	**Amount adsorbed (mg g^{-1})**
1	129
2	127
3	120
Average	**125**
RSD	**3.7%**

ATR-FTIR was employed to assess the repeatability of the PEGMA$_{950}$ grafting. To account for variability in the mass of material being characterized all spectra were normalized (0,1). Two batches were assessed, for batch 1 three points across the material were measured (n=3) to assess intra batch grafting variability.

Table S8 Normalized peak area for the 1114 cm^{-1} (ether functional group) of the PDVB-g-$PEGMA_{950}$

Sample	**Area**	**% RSD**
Batch 1.1	26.28	1.27
Batch 1.2	28.14	4.99
Batch 1.3	24.30	2.49
Batch 2	26.23	N/A
Average	**26.24**	
RSD	**% 5.97**	